Optics Communications 461 (2020) 125258

Contents lists available at ScienceDirect

Optics Communications

journal homepage: www.elsevier.com/locate/optcom

Influences of nanosecond pulse pre-irradiation on femtosecond laser damage resistance of gold pulse compression grating

Yuchen Shao [a,b,c], Yuan'an Zhao [a,c,d,*], Hao Ma [a,b,c], Cheng Li [a,b,c], Dawei Li [a,c], Cheng Wang [e], Yuxin Leng [e], Jianda Shao [a,c]

[a] Laboratory of Thin Film Optics, Shanghai Institute of Optics and Fine Mechanics, Shanghai 201800, China
[b] Center of Materials Science and Optoelectronics Engineering, University of Chinese Academy of Sciences, Beijing 100049, China
[c] Key Laboratory of Materials for High Power Laser, Chinese Academy of Sciences, Shanghai 201800, China
[d] State Key Laboratory of Applied Optics, Changchun Institute of Optics, Fine Mechanics and Physics, Chinese Academy of Sciences, Changchun 130033, China
[e] State Key Laboratory of High Field Laser Physics, Shanghai Institute of Optics and Fine Mechanics, Chinese Academy of Sciences, Shanghai 201800, China

ARTICLE INFO

Keywords:
Femtosecond laser damage
Gold-coated pulse compression gratings
Nanosecond pre-pulse
Bidirectional grating compressor
Nano- and femtosecond dual beam processing

ABSTRACT

The gold pulse compression gratings (PCG) used in the Bidirectional Grating Compressor (BGC) suffers a nano- and femtosecond dual pulses irradiation. In the case that the ns pre-pulse comes 10 nanoseconds early before the fs pulse, experiments were conducted to investigate damage behaviors under the dual pulse irradiation. 1-on-1 laser induced damage threshold (LIDT) of the ns–fs dual pulses and fs single pulse were tested and compared. Scanning Electron Microscope (SEM) was employed to capture damage onset and exam the damage macro- and micro-morphologies. The mono-shot method, comparison between the damage zone and spatial distribution of laser pulses, was employed to analyze the difference of the damage onset fluences for the two cases thoroughly. It was found that there is no degradation of laser damage resistance due to the ns pre-pulse. Instead, a slightly increase (~10%) of fs LIDT caused by the ns pre-pulse was found.

1. Introduction

Nano- (ns) and femtosecond (fs) dual beam processing are broadly used in various regions, such as enhanced laser micro-machining [1–3], material removal [4], laser filaments [5] and so on. In most of these application scenarios, fs ablation/damage/removal of different materials (dielectrics/metal/silica) is enhanced due to the ns pre-pulse irradiation. Lin et al. has reported that when there is a nanosecond pre-pulse 30 ns ahead, fused silica [1] and aluminum [4] sample are ablated more by the fs pulse. Kerrigan et al. has also observed that laser filaments on GaAs are enhanced with fs–ns pulse pairs [5]. The ns laser can also help to increase the resolution of micro-lithology via stimulated emission depletion (STED) [2,3]. Also, the Bidirectional Grating Compressor (BGC) [6], designed for Shanghai Superintense Ultrafast Laser Facility (SULF), provides a specific irradiation condition of ns–fs dual laser pulse on the gold pulse compression grating (PCG). Interestingly, the femtosecond damage of gold PCG was relieved instead of being enhanced by the nanosecond pulse based on experiment and analysis.

The gold PCG is prone to be damaged but necessary as a dispersion element [7,8] in the CPA [9,10] for its broadband high efficiency. And the laser damage resistance of gold PCG greatly limits the output power of the CPA system. In order to avoid its laser damage problem, large-size gratings are commonly required to reduce the energy density irradiating on the surface. However, it challenges the fabrication processing of large-size gratings and the quality of beam transmission [11,12]. Therefore, the BGC has been designed to avoid the aforesaid problems by halving the energy density [6]. The schematic diagram of the BGC is shown in Fig. 1. After splitting with a ratio of 1:1, two identical nanosecond laser pulses (a1 and a2) are delivered into the BGC. After stretching and the compression in two opposite directions, two compressed femtosecond pulses out of the BGC remain accurate synchronization and reach the destination simultaneously. Compared with traditional one-directional grating compressors, gratings of the BCG (g1, g4) suffers only a half of the energy density of compressed femtosecond pulse with the unaltered irradiated area. Without changing the laser safe operation fluence of gold PCGs, the BGC can theoretically double the output energy.

But for the gold PCG g1, it suffers not only a halved fs pulse (the compressed a2) but also a ns pre-pulse (the uncompressed a1). The time delay between the ns pre-pulse and the fs pulse is about 30 ns due to the extra optical path of a1. The fluence ratio of the femtosecond to nanosecond pulse is 3:4. It has been demonstrated that the LIDT of gold

* Correspondence to: Laboratory of Thin Film Optics, Shanghai Institute of Optics and Fine Mechanics, No.390 Qinghe Road, Jiading District, Shanghai 201800, China.
E-mail addresses: yazhao@siom.ac.cn (Y. Zhao), jdshao@siom.ac.cn (J. Shao).

https://doi.org/10.1016/j.optcom.2020.125258
Received 13 October 2019; Received in revised form 2 January 2020; Accepted 4 January 2020
Available online 9 January 2020
0030-4018/

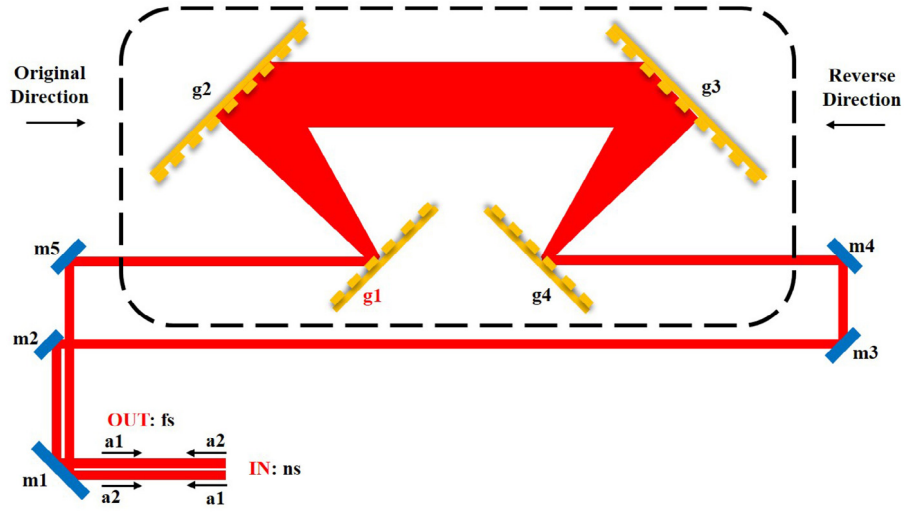

Fig. 1. The schematic diagram of the BGC. The gold grating g1 is the prototype of gold PCG we investigate in this paper. It suffers an uncompressed nanosecond laser pulse ~30 ns prior to a compressed femtosecond pulse.

PCGs is around 0.2 J/cm^2 to femtosecond pulse and above 0.4 J/cm^2 to nanosecond pulse width [13–16]. Therefore, the ns–fs dual pulses irradiation is a new condition for investigation of the laser damage behavior of gold PCGs.

Generally, damage of gold gratings (films) caused by the pulsed laser is considered to be associated with thermal process of its electron–lattice system [14,17–20]. The process is often simulated by One- and Two-Temperature Model (TTM) for the nano- and femtosecond cases, respectively [21–26]. For the ns pre-pulse, without damaging the PCG, the electron–lattice system could still be heated. The thermal absorption and cooling take about tens of nanoseconds [21,25], which is in the same magnitude of the interval between the ns pre-pulse and fs pulse [6]. It is questionable whether the heat caused by ns pre-pulse could relax completely before the fs post-pulse comes. A longer interval (>100 ns) makes the ns pre-pulse and the fs post-pulse independent. Whereas, the shorter interval (<50 ns), with residual heat caused by the ns pre-pulse, will enhance the fs damage behavior theoretically. For the fs pulse, electron gas of the gold layer absorbs laser energy first; then the lattice is heated via electron–phonon coupling [22,23]. If the temperature does not return to the ambient value, the electron–lattice system will obtain a higher initial temperature according to the TTM of fs case; meanwhile, strength of electron–phonon coupling also increases with the increasing electron temperature [26]. Both factors will lead to a higher peak temperature of the lattice in hundreds of picoseconds [14,24,25], which means an enhanced damage behavior of the PCG.

Besides aforementioned possible pre-heated effects, it has been reported that the femtosecond laser-material interaction could be enhanced by the nanosecond pre-pulse. Chen et al. has been reported that the nanosecond pre-irradiation can reduce the femtosecond laser damage resistance of Ta_2O_5/SiO_2 high reflectors via the contribution of electron defects [27]. Femtosecond ablation of fused silica/aluminum /GaAs has been observed to be enhanced due to a ns pre-pulse ahead of tens of nanosecond [1,4,5]. To our knowledge, no laser-induced damage threshold (LIDT) investigation of gold PCGs under similar conditions has been published yet. Considering these possible negative effects caused by the nanosecond pre-pulse, it is instructive to measure the LIDT of gold PCGs under the ns–fs dual pulses irradiation of the BGC.

In this paper, we designed a dual pulses damage testing setup based on a commercial Ti: Sapphire laser system. The dual pulses damage resistance of the gold PCG was evaluated by the 1-on-1 method, and the LIDT of fs single pulse was also tested for comparison. The experimental method is described detailly in Section 2. Results of LIDTs are shown in Section 3. It is found that there is no degradation of the femtosecond LIDT due to the nanosecond pre-irradiation. Instead, laser damage behavior of the fs pulse seems to be relieved slightly by the nanosecond pre-pulse. Sizes of damage spots were measured to evaluate the relief macroscopically. The mono-shot method, establishing a correspondence between the damage morphology and local fluence, has been employed to analyze differences of the damage onset fluences for the two cases thoroughly, and the slightly increase due to the nanosecond pre-pulse are shown in Section 4. In summary, the femtosecond laser safe operational limit of the gold PCG operating in BGC will not be reduced by the nanosecond pre-pulse. Nanosecond pre-irradiation shows its potential to protect the easily damaged elements operated in high power laser systems.

2. Experimental method

2.1. Sample

The sample grating is a small version of the gold PCG g1 operating in the BGC. The 1480 gr/mm gold grating is coated on a 40 × 60 mm pyrex substrate with periodic micro-structures. The 1st diffraction efficiency of the sample is higher than 90% in the measuring wavelength range of 750–850 nm. Surface of the sample was rushed by airflow before testing.

2.2. Experimental setup

Fig. 2 is the schematic diagram of the testing platform. The Ti: Sapphire laser system (Spectra Physics Spitfire Ace, 10 Hz), based on the CPA, contains three assemblies: a Stretcher, a Ti: Sapphire Regenerative Amplifier and a Compressor. The seed pulse (35 fs, 550 mW, 80 MHz) was imported into the Stretcher and the Regenerative Amplifier to obtain a 1-ns pulse with the energy of 3.2 mJ. Half of the 1-ns pulse was taken out directly and focused on the sample. Then the other half of the 1-ns pulse was delivered to the Compressor to export a 120-fs pulse with the energy of 1.8 mJ. The 120-fs pulse was delayed 10 ns to the sample by extra optical path with the two folding mirrors M1 and M2. Considering of beam quality deterioration after long-distance transportation (about 10 meters between M1 and M2 in Fig. 2 for 30 ns delay), the actual time delay of 10 ns was chosen for the test. The shortened time delay will not affect the aforementioned mechanism. This time delay was measured by a photoelectric detector

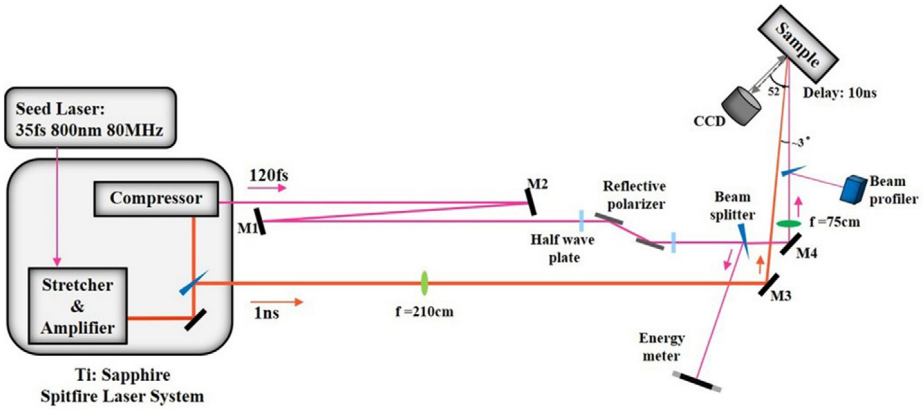

Fig. 2. LIDT testing setup. M1–M4 are the reflection mirrors.

and an oscilloscope. Pulse widths were measured by an autocorrelator (Minioptic, Delta AC) before testing.

For the 120-fs pulse, its attenuation and p-polarization were realized through half wave plates and reflective polarizers. The pulse energy was measured and recorded by an energy meter (EnergyMax-USB, Coherent) through a 4% beam splitter (BS). The beam was focused onto the sample surface by a lens with the focal length of 75 cm and produced a 0.045 mm^2 effective focal spot perpendicular to the propagation axis. The focused beam was split through another 4% BS, and the focal spot was monitored by a beam profiler (BeamView-USB, Coherent). The pixel of the beam profiler is 6.7 μm × 6.7 μm. The fluence of the 120-fs pulse was diagnosed and recorded by the energy meter and beam profiler in-situ. For the 1-ns pulse, the beam was operated at the TEM_{00} mode and focused onto the sample by a lens with the focal length of 210 cm. Effective area of its focal spot perpendicular to the propagation axis was 0.17 mm^2. Without in-situ diagnose, the energy and focal spot of the 1-ns pulse were measured and fixed before testing. The ns spot size is almost three times as large as the fs spot size, so the fs spot could be located at the center of the ns spot conveniently. So that we can bypass the effect of the distribution of the ns fluence as much as possible. A CCD camera with suitable attenuation was placed at the target plane to make sure this overlap of the two focal spots.

The sample grating was positioned on a motorized x–y translation stage. The incident angles of the 1-ns and 120-fs laser beam were 49° and 52°, respectively.

2.3. Test procedure

The LIDT test mode was "1-on-1" according to ISO21254-1 [28]. In this paper, all the fluences are given by:

$$F = \frac{E}{A_{eff}/\cos\alpha} \tag{1}$$

where E is the energy of the laser pulse. A_{eff} is the effective area of the focal spot perpendicular to the propagation axis. α is the incident angle of the laser beam. F is the fluence and F_{th} is the 0% probability LIDT of the sample. The damage is defined to be a visible change in the surface morphology under the off-line SEM.

Under the 1-on-1 mode, we devised three steps to investigate the LIDT comparison between fs single pulse irradiation (120-fs pulse) and ns–fs dual pulses irradiation (1-ns pulse 10 nanosecond prior to 120-fs pulse). The durations followed the conditions in the BGC device [6,29]. The highest output fluence of the 120-fs pulse of the setup was 0.45 J/cm^2. Considering the fluence ratio of the fs pulse to the ns pulse is 3:4 in the BGC, the fluence of the 1-ns pulse was adjusted to 0.62 J/cm^2 by lens with a focal length of 210 cm. Firstly, we tested and found that there was no damage on the sample after the 1-ns pulse irradiation with the fluence of 0.62 J/cm^2. The 1-ns pulse was considered as a pre-pulse in the test of ns–fs dual pulses irradiation. Secondly, the LIDT of the fs single pulse was tested. Finally, the LIDT of ns–fs dual pulses with an interval of 10 nanosecond was tested for comparison.

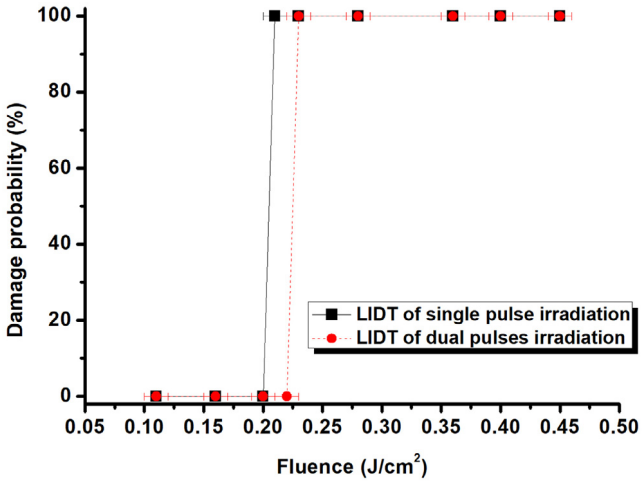

Fig. 3. LIDT of fs single pulse (square) and ns–fs dual pulses (circle). Each data point represents 10 shots with a fluence error of ±0.01 J/cm^2.

3. LIDT results

First of all, there was no damage under the 1-ns pulse irradiation with the fluence of 0.62 J/cm^2. Fig. 3 depicts the different LIDT results of fs single pulse and ns–fs dual pulses. The LIDT of the 120-fs pulse is 0.20 ± 0.01 J/cm^2 and the LIDT of dual pulses irradiation is 0.22 ± 0.01 J/cm^2. The fluences corresponding to the 0% and 100% probability are close. It is common for the femtosecond pulse to have sharp damage probability curves [13]. Each data point represents ten shots. The error bar of ±0.01 J/cm^2 is due to statistic. LIDTs of the two cases seem to border error bars of each other. The increase of the fs LIDT due to the ns pre-irradiation is supported by the following damage morphology analysis.

4. Discussions

4.1. Typical damage morphologies of the two cases

Fig. 4 shows typical morphologies of the grating photographed by SEM. The pristine surface morphology of the grating without any laser irradiation is shown in Fig. 4(a). The original surface shows

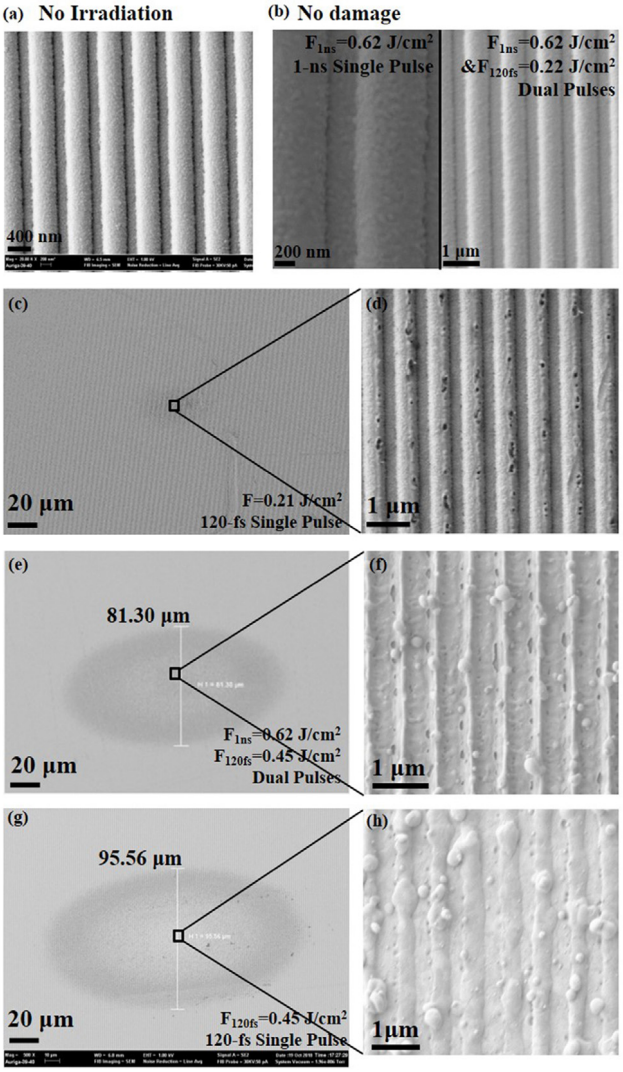

Fig. 4. SEM images of typical surface morphology of the grating under different irradiation conditions. (a) Pristine surface morphology without laser irradiation. (b) Undamaged morphology of 1-ns pulse (left) and dual pulses irradiation (right). (c) (d) Damage morphology near the LIDT of 120-fs single pulse. (e) (f) and (g) (h) Damage morphology under the two kinds of irradiation when the fluence of the 120-fs pulse is 0.45 J/cm^2.

a clear boundary between the ridges and grooves. The undamaged morphologies of the two kinds of irradiation are shown in Fig. 4(b). After the 1-ns pulse irradiation with the fluence of 0.62 J/cm^2, no damage was observed under a 50,000× magnification (Fig. 4(b) left side).

The damage morphology at the fluence very near to the LIDT was examined carefully. Fig. 4(b) also shows that no damage occurs under ns–fs dual pulses irradiation when the fluence of fs pulse is 0.22 J/cm^2. However, damage appears as discrete small sunk pits facing to the incident laser appears on the right side of the ridges after fs single pulse irradiation with the fluence of 0.21 J/cm^2 (Fig. 4(c) and (d)). The widths of these pits are from several nm to tens of nm. And the pits connect together to form a line on the ridge. The occurrence of the initial damage requires a higher fluence of the fs pulse in the case of dual pulses irradiation.

The damage morphology at the highest fluence of the 100% LIDT was also compared. Fig. 4(e) and (g) exhibit a conspicuous comparison of damage areas between the two cases when the fluence of the fs pulse is 0.45 J/cm^2. The damage area of fs single pulse is larger than

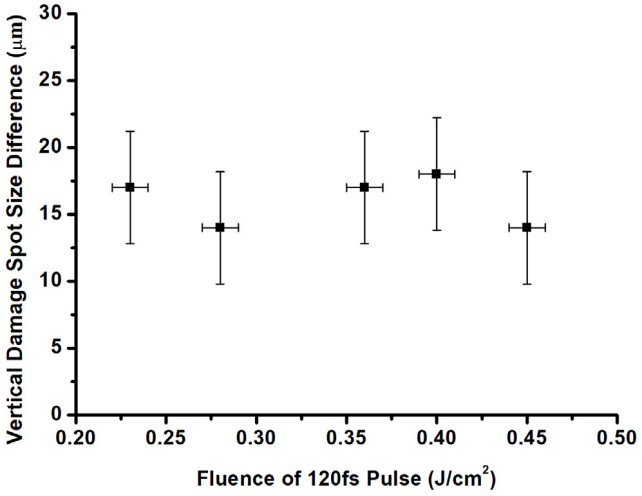

Fig. 5. Difference of the vertical damage spot size between the two kinds of irradiation. Each data point is with a fluence error of ±0.01 J/cm^2 and a difference value error of ± 4.2 μm, respectively.

the one of ns–fs dual pulses. In Fig. 4(f), ridges of the grating melts at the center of the damage area, and the molten gold spackles to the grooves. For comparison, the whole gold coating at the center of damage area appears as melting and resolidification on the substrate under irradiation of fs single pulse with the fluence of 0.45 J/cm^2 in Fig. 4(h). The 120-fs laser damage behavior of the gold grating is relieved slightly by the 1-ns pre-pulse. The overall damage area is elliptical due to oblique incidence.

Though the LIDT values of the two cases seems to be within the error bars of each other, the comparison between the two cases indicates that the 1-ns pre-pulse has relieved femtosecond laser damage behaviors to some extent. Fig. 4(e) and (g) show that the damage spot is larger without the 1-ns pre-pulse. To evaluate the relief due to the 1-ns pre-pulse, the level of damage was quantified macroscopically based on the vertical damage spot size. The vertical damage spot sizes of the two cases were measured under the SEM with an error of ±3 μm. Their difference is obtained via subtracting the vertical damage spot size of the ns–fs case from the fs case. Considering of the propagation of error, the error of the difference is ± 4.2 μm ((3^2+3^2)^0.5). Fig. 5 shows the difference when the fs fluence are the same. Differences with various fs fluence are at the same level in general. The relatively uniform difference indicates that the relief of fs LIDT due to the 1-ns pre-pulse is independent of the fluence distribution of 1-ns pre-pulse. This may attribute to the much larger focal spot of the ns pulse than the fs pulse (Fig. 6(b)). Besides, based on the mono-shot method, the relief is anatomized with more morphology details in the following.

4.2. Mono-shot analysis and discussion

Thanks to the near Gaussian profile of the focal spot, the planar distribution of fluence on sample surface is a near Gaussian profile, too. A correspondence between damage area and local fluence of the focal spot can be obtained via recording the profile of the beam and the energy of the pulse. The location just outside the edge of the damaged area corresponds to the maximum fluence to avoid triggering the damage, as the so-called 0% probability LIDT. The mono-shot method has been successfully utilized in precise determination of LIDT and analysis of laser-induce damage [30,31]. In this discussion, the mono-shot method is applied to quantify the relationship between the variation of damage behaviors and the increasing fluence of the fs pulse. In the two cases, fs pulse and ns–fs dual pulses irradiation, the relationship is established on y-axis. Differences of the damage

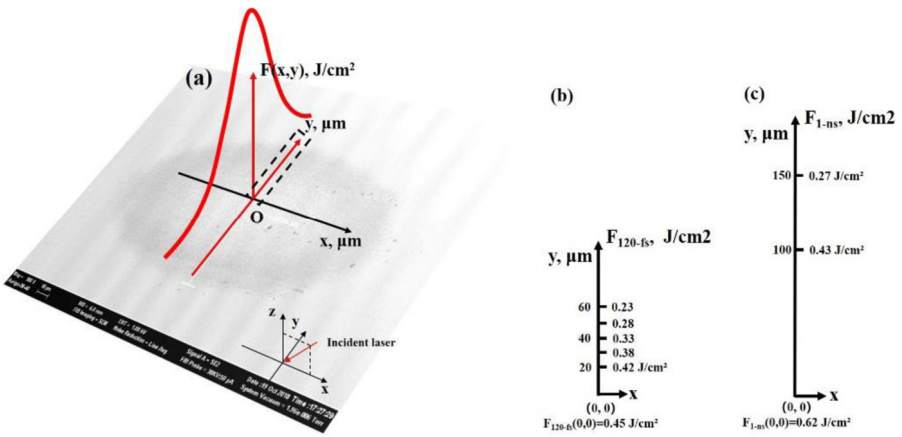

Fig. 6. (a) Schematic diagram of the fluence distribution on the PCG surface. The details of damage discussed later are extracted from the dash rectangle, which is a relative location in the Gaussian profile. (b) and (c) Fluence distributions of the 120-fs and 1-ns pulse on y-axis, respectively.

morphology of the two cases are analyzed thoroughly at the highest fluence of the 100% LIDT for its apparent phenomenon.

For a certain pulse, the fluence distribution on the sample surface is given by

$$F(x,y) = F_0 \times \exp(-2\frac{x^2}{{\omega_x}^2}) \times \exp(-2\frac{y^2}{{\omega_y}^2}) \quad (2)$$

where $F(x,y)$ is the fluence of the selected location, and (x,y) is the coordinate of it. F_0 is the peak fluence at position (0, 0). ω_x and ω_y are the radius of long axis and short axis due to the oblique incidence. To simplify the analysis, damage region along y-axis (y > 0) is extracted to analyze. Eq. (2) can be reduced to:

$$F(0,y) = F_0 \times \exp(-2\frac{y^2}{{\omega_y}^2}), x = 0 \quad (3)$$

Fig. 6(a) is a schematic diagram of the laser fluence distribution on the PCG surface, and the dash rectangle is the region for analysis. The fluence distributions of the 120-fs pulse with the peak fluence of 0.45 J/cm^2 and the 1-ns pulse with the peak fluence of 0.62 J/cm^2 are shown in Fig. 6(b) and (c), respectively. In this paper, the 120-fs and 1-ns laser beams were both incident from the right side of Fig. 6(a).

The two strip images in Fig. 7 are the enlargement of the dash rectangle damage region in Fig. 6(a). Typical damage morphologies of gold grating under 120-fs pulse with the peak fluence of 0.45 J/cm^2 are shown in Fig. 7(a). On the top of Fig. 7(a), initial damage appears as discrete distribution of small sunk pits on the right side of grating ridges, while the grooves and the other side of ridges keep unchanged after irradiation (0.21–0.27 J/cm^2). As the fluence increasing (0.27–0.37 J/cm^2) the ridges are ablated more, and the small sunk pits extend laterally from the right to the left side of the ridges. The transformative ridges gradually spread to the grooves on both sides. With a higher fluence (0.37–0.40 J/cm^2), the ridges show like melting, then resolidify and fill into the grooves. When the fluence is above 0.40 J/cm^2, there are even some solidified beads with an about 0.5-μm diameter on the PCG surface. The gold-coating is melted as a whole, and the period micro-structures still exists under the melting coating. For comparison, damage morphologies under ns–fs dual pulses irradiation are shown in Fig. 7(b). Though the evolution of damage versus fluence increasing is similar to the case of 120-fs single pulse, there are still some differentiate: (1) The initial small sunk pits appears when the fluence of the fs pulse reaches 0.23 J/cm^2. (2) To reach an equivalent damage morphology, it needs a fluence increment of ~0.03 J/cm^2 higher than the case of fs single pulse. (3) Even the fluence of the fs pulse is above 0.40 J/cm^2, there are very few small resolidified beads. And the gold coating is not melted totally. In a way, the ns pre-pulse was proved to relieve the damage behavior of the fs pulse.

4.3. Discussion for underlying reasons of the relief

Though the 1-ns pre-pulse could heat the gold surface of the grating. Thermal process existing in the surface may bring some positive influences rather than damage it, such as the cleaning effect [32,33] or annealing effect [34]. Both the two effects can make the gold surface smoother.

As a period micro-structure element, surface of the grating can absorb impurities (oxygen, oil and so on) during production, storage, transportation and service [35,36]. Contaminants deposition on the sample will lead to grating lines absences or added nodule, which are known to cause electric-field enhancement in the shallow layer of the gold layer and reduce the laser damage resistance [37,38].

The so-called laser cleaning effect could remove the oxygen via laser assisted reduction reactions, and separate other contaminants via thermal stress caused by the laser pulse. When the surface of the gold layer absorbs energy of the laser pulse and heat up, the contaminants could also heat up at the same time. A shockwave could propagate from the surface to contaminants. When the thermal stress is higher than their binding force between contaminants and the surface, the contaminants will be separated from the surface [36,39]. The slight difference between the LIDT results of two cases meets this effect in a way. But the mechanism of nanosecond pre-irradiation still needs to be studied in the future work.

5. Conclusion

In the region of ns–fs dual beam processing, most of the materials are ablated/removed more due to the coupling of ns and fs pulse. In BGC, however, the extra nanosecond pre-irradiation will not reduce the femtosecond laser safe operational fluence of the gold PCG. With the 1-ns pre-pulse irradiation, the fs LIDT of the gold PCG is slightly increased from 0.20 ± 0.01 to 0.22 ± 0.01 J/cm^2 (~10%) via the 1-ns pre-pulse, and the damage sizes become smaller. Underlying reasons of the increase have been discussed. Though the mechanism of the LIDT increase needs further work to be validated, nanosecond pre-irradiation is expected to be a potential method to relieve the laser damage behaviors of other optical elements operated in high power laser systems.

CRediT authorship contribution statement

Yuchen Shao: Investigation, Methodology, Validation, Writing - original draft. **Yuan'an Zhao:** Resources, Writing - review & editing, Funding acquisition. **Hao Ma:** Validation. **Cheng Li:** Validation. **Dawei Li:** Investigation, Methodology. **Cheng Wang:** Investigation, Methodology, Resources. **Yuxin Leng:** Resources. **Jianda Shao:** Resources, Writing - review & editing, Funding acquisition.

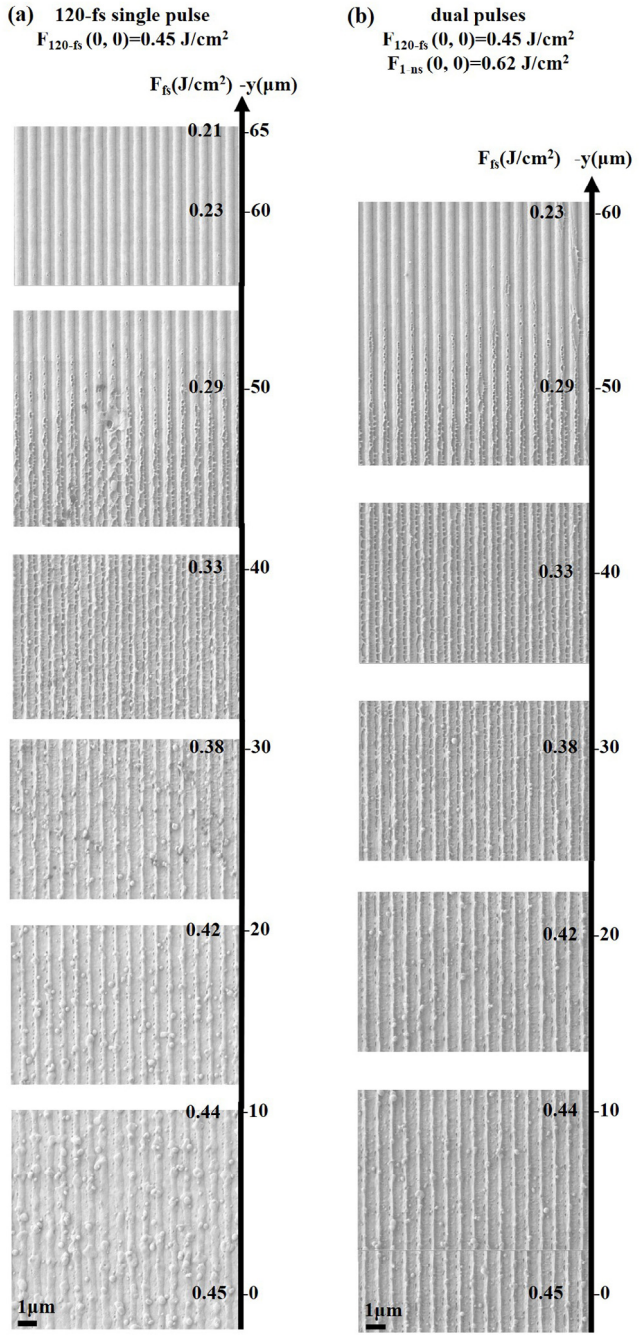

Fig. 7. Jigsaw of SEM images shows comparison of damage morphologies on *y*-axis (y > 0) between the two cases. (a) and (b) are damage behaviors of 120-fs single pulse and ns–fs dual pulse. The fluence of the 120-fs and 1-ns pulse was 0.45 J/cm^2 and 0.62 J/cm^2, respectively.

Funding

This research was supported by National Natural Science Foundation of China (Grant No. 11874369 and U1831211) and Strategic Priority Research Program of the Chinese Academy of Sciences (Grant No. XDB1603).

References

[1] C.-H. Lin, Z.-H. Rao, L. Jiang, W.-J. Tsai, P.-H. Wu, C.-W. Chien, S.-J. Chen, H.-L. Tsai, Investigations of femtosecond-nanosecond dual-beam laser ablation of dielectrics, Opt. Lett. 35 (2010) 2490–2492.
[2] R. Wollhofen, J. Katzmann, C. Hrelescu, J. Jacak, T.A. Klar, 120 nm resolution and 55 nm structure size in STED-lithography, Opt. Express 21 (2013) 10831–10840.
[3] J. Fischer, J.B. Mueller, A.S. Quick, J. Kaschke, C. Barner-Kowollik, M. Wegener, Exploring the mechanisms in STED-enhanced direct laser writing, Adv. Opt. Mater. 3 (2015) 221–232.
[4] C.-H. Lin, Z.-H. Rao, L. Jiang, W.-J. Tsai, P.-H. Wu, C.-W. Chien, H.-L. Tsai, Enhancement of ablation efficiency by a femto/nano-second dual-beam micromachining system, SPIE (2010).
[5] H. Kerrigan, S.R. Fairchild, M. Richardson, Nanosecond laser coupling for increased filament ablation, Opt. Lett. 44 (2019) 2594–2597.
[6] C. Wang, Z. Li, S. Li, Y. Liu, Y. Leng, R. Li, Bidirectional grating compressors, Opt. Commun. 371 (2016) 248–251.
[7] N. Bonod, J. Neauport, Diffraction gratings: from principles to applications in high-intensity lasers, Adv. Opt. Photonics 8 (2016) 156–199.
[8] H. Guan, H. Chen, J. Wu, Y. Jin, F. Kong, S. Liu, K. Yi, J. Shao, High-efficiency, broad-bandwidth metal/multilayer-dielectric gratings, Opt. Lett. 39 (2014) 170–173.
[9] D. Strickland, G. Mourou, Compression of amplified chirped optical pulses, Opt. Commun. 55 (1985) 447–449.
[10] W. Li, Z. Gan, L. Yu, C. Wang, Y. Liu, Z. Guo, L. Xu, M. Xu, Y. Hang, Y. Xu, 339 J high-energy Ti: sapphire chirped-pulse amplifier for 10 PW laser facility, Opt. Lett. 43 (2018) 5681–5684.
[11] L. Shi, L. Zeng, L. Li, Fabrication of optical mosaic gratings with phase and attitude adjustments employing latent fringes and a red-wavelength dual-beam interferometer, Opt. Express 17 (2009) 21530–21543.
[12] E.-C. Chang, D. Mikolas, P.-T. Lin, T. Schenk, C.-L. Wu, C.-K. Sung, C.-C. Fu, Improving feature size uniformity from interference lithography systems with non-uniform intensity profiles, Nanotechnology 24 (2013) 455301.
[13] P. Poole, S. Trendafilov, G. Shvets, D. Smith, E. Chowdhury, Femtosecond laser damage threshold of pulse compression gratings for petawatt scale laser systems, Opt. Express 21 (2013) 26341–26351.
[14] Z. Xia, H. Huang, F. Kong, L. Wang, Y. Jin, Varied laser induced damage phenomena of gold coated gratings for pulse compression, Opt. Lasers Eng. 95 (2017) 42–51.
[15] H. Huang, L. Wang, F. Kong, Z. Xia, Y. Jin, J. Xu, J. Chen, Y. Cui, J. Shao, Effects of substrate on the femtosecond laser-induced damage properties of gold films, Opt. Mater. 81 (2018) 115–121.
[16] F. Kong, H. Huang, L. Wang, J. Shao, Y. Jin, Z. Xia, J. Chen, L. Li, Femtosecond laser induced damage of pulse compression gratings, Opt. Laser Technol. 97 (2017) 339–345.
[17] Y. Zhang, J. Chen, Melting and resolidification of gold film irradiated by nano-to femtosecond lasers, Appl. Phys. A 88 (2007) 289–297.
[18] L. Zhou, L. Li, Melting and resolidification of gold film irradiated by laser pulses less than 100 fs, Appl. Phys. A 116 (2014) 2157–2165.
[19] J. Krüger, D. Dufft, R. Koter, A. Hertwig, Femtosecond laser-induced damage of gold films, Appl. Surf. Sci. 253 (2007) 7815–7819.
[20] G. Du, F. Chen, Q. Yang, J. Si, X. Hou, Ultrafast temperature relaxation evolution in au film under femtosecond laser pulses irradiation, Opt. Commun. 283 (2010) 1869–1872.
[21] N.M. Bulgakova, A.V. Bulgakov, Pulsed laser ablation of solids: transition from normal vaporization to phase explosion, Appl. Phys. A 73 (2001) 199–208.
[22] B. Rethfeld, A. Kaiser, M. Vicanek, G. Simon, Ultrafast dynamics of nonequilibrium electrons in metals under femtosecond laser irradiation, Phys. Rev. B 65 (2002) 214303.
[23] B. Rethfeld, K. Sokolowski-Tinten, D. von der Linde, S.I. Anisimov, Ultrafast thermal melting of laser-excited solids by homogeneous nucleation, Phys. Rev. B 65 (2002) 092103.
[24] D.S. Ivanov, L.V. Zhigilei, Combined atomistic–continuum modeling of short-pulse laser melting and disintegration of metal films, Phys. Rev. B 68 (2003) 064114.
[25] N.M. Bulgakova, A.V. Bulgakov, L.P. Babich, Energy balance of pulsed laser ablation: thermal model revised, Appl. Phys. A 79 (2004) 1323–1326.
[26] Z. Lin, L.V. Zhigilei, V. Celli, Electron–phonon coupling and electron heat capacity of metals under conditions of strong electron–phonon nonequilibrium, Phys. Rev. B 77 (2008) 075133.
[27] S. Chen, Y.a. Zhao, D. Li, H. He, J. Shao, Effect of nanosecond laser pre-irradiation on the femtosecond laser-induced damage of Ta 2 O 5/SiO 2 high reflector, Appl. Opt. 51 (2012) 1495–1502.
[28] ISO standard nos. 21254-1–21254-4, 2011.
[29] Y. Chen, C. Wang, Z. Zhang, X. Yang, Y. Xu, Y. Leng, Z. Xu, Investigation of spatio-temporal stretching in a duplex grating compressor, Opt. Express 27 (2019) 31667–31675.
[30] M. Sozet, J. Neauport, E. Lavastre, N. Roquin, L. Gallais, L. Lamaignère, Assessment of mono-shot measurement as a fast and accurate determination of the laser-induced damage threshold in the sub-picosecond regime, Opt. Lett. 41 (2016) 804–807.
[31] S. Elhadj, J.H. Yoo, Efficient method for the measurement of lifetime optical damage performance of thin film coatings from laser damage size analysis, Opt. Lett. 42 (2017) 3153–3156.

[32] A.C. Tam, W.P. Leung, W. Zapka, W. Ziemlich, Laser-cleaning techniques for removal of surface particulates, J. Appl. Phys. 71 (1992) 3515–3523.
[33] Y. Ye, X. Yuan, X. Xiang, M. Chen, X. Miao, H. Lv, H. Wang, C. Wang, W. Zheng, CO2 laser-cleaning of dimethylsilicone contamination on the surface of gold films, SPIE (2009).
[34] Y. Chen, J. Wang, X. Chen, M. Yan, M. Qiu, Plasmonic analog of microstrip transmission line and effect of thermal annealing on its propagation loss, Opt. Express 21 (2013) 1639–1644.
[35] E. Gubbini, G. Kommol, M. Schnürer, H. Schönagel, U. Eichmann, M.P. Kalashnikov, P.V. Nickles, F. Eggenstein, G. Reichardt, W. Sandner, On-line cleaning of optical components in a multi-TW-Ti:Sa laser system, Vac. 76 (2004) 45–49.
[36] T. Jitsuno, H. Murakami, S. Motokoshi, E. Saato, K. Mikami, K. Kato, T. Kawasaki, Y. Nakata, N. Sarukura, T. Shinizu, H. Shiraga, N. Miyanaga, H. Azechi, Oil-contamination problem in large-scale pulse-compressor, SPIE (2010).
[37] A.E. Wynne, B.C. Stuart, Rate dependence of short-pulse laser ablation of metals in air and vacuum, Appl. Phys. A 76 (2003) 373–378.
[38] Y. Jin, H. Guan, F. Kong, J. Wang, A. Erdmann, S. Liu, Y. Du, J. Shao, H. He, K. Yi, Influence of two typical defects on the near-field optical properties of multilayer dielectric compression gratings, Appl. Opt. 51 (2012) 6683–6690.
[39] J.-M. Lee, J.-E. Yu, Y.-S. Koh, Experimental study on the effect of wavelength in the laser cleaning of silver threads, J. Cult. Herit. 4 (2003) 157–161.